Mutual Segmentation with Level Sets

Tammy Riklin-Raviv   Nir Sochen   Nahum Kiryati

Tel Aviv University, Tel Aviv 69978, Israel

tammy@eng.tau.ac.il   sochen@post.tau.ac.il   nk@eng.tau.ac.il

Abstract

We suggest a novel variational approach for mutual segmentation of two images of the same object. The images are taken from different views, related by projective transformation. Each of the two images may not provide sufficient information for correct object-background delineation. The emerging segmentation of the object in each view provides a dynamic prior for the segmentation of the other image. The foundation of the proposed method is a unified level-set framework for region and edge based segmentation, associated with a shape similarity term. The dissimilarity between the two shape representations accounts for excess or deficient parts and is invariant to planar projective transformation. The suggested algorithm extracts the object in both images, correctly recovers its boundaries, and determines the homography between the two object views.

1. Introduction

Object segmentation is challenging in the presence of noise, shadowing, saturation or occlusion. Hence, the commonly used edge-based or region-based segmentation techniques are insufficient. Prior knowledge on the object of interest could facilitate the segmentation process, but such information is usually limited.

Consider the segmentation of two images of the same object. In many cases, each image by itself cannot be correctly segmented, hence background regions can be mistakenly labeled as foreground (excess) or vice versa (deficiency). Had good segmentation been possible in either image, it could have been used as a prior for the other. Since this is not possible due to the poor segmentation of each image by itself, we propose *mutual segmentation* of the two object views, using each evolving contour to support the extraction of the other.

Mutual segmentation benefits from the availability of different object views. However, concurrent processing of an image pair requires object registration. We address concurrent segmentation and registration of two object views related by planar projective transformation.

We use the level set framework for segmentation [17] where images are represented via level-set functions. The representation of shape via the positive levels of the image level-set function is parameterization-free, enabling meaningful definition of shape dissimilarity measures between object views. Moreover, any transformation applied on the image changes the coordinate system of its level-set function. The represented shape is thus transformed correspondingly, simplifying the process of shape alignment.

In variational image segmentation methods, the optimal delineating object boundaries are inferred by minimizing a cost functional that constrains the compatibility of the evolving contour with the image data while restricting its length and smoothness. See [1] and references therein. Top-down approaches incorporate prior knowledge to facilitate the segmentation of occluded or noisy images. Model-based methods impose additional constraints that relate to typical attributes of the particular class of objects. Refer for example to [9] that extracts thin structures such as blood vessels or to [21] that incorporates geometric information to segment road networks. When the object shape is specified, resemblance of the segmented object to the reference shape can be also promoted. Prior-based segmentation methods [6, 7, 19, 20, 22] assume the existence of a well-defined shape prior and use it to extract the obscure object boundaries. The Statistical approaches [4, 5, 10, 14, 22, 25] capture possible shape variability by employing a set of similar but not identical shape priors. These methods, however, depend on the availability of a comprehensive set of priors or a segmented instance of the object of interest.

The mutual segmentation approach goes beyond the concepts of prior-based segmentation because a well-defined prior is not available and the matching is between two possibly corrupted and noisy images. The main difficulty resides in labeling regions where the aligned images do not overlap. Obviously, erroneous foreground-background classifications undesirably spoil the segmentations of both images. Paraphrasing an old urban legend, would an hypothetic child of Marilyn Monroe and Albert Einstein necessarily be genius and beautiful? The conflict between two possible interpretations of mutually segmented images has

never been addressed before. In [8] a majority rule is applied to complete the missing contour parts in a set of similar shapes. The method of [28] handles only pairs of noisy images, where at least one of the images nearly contains sufficient information to be segmented by itself. The ambiguity induced by a concurrent segmentation of an image pair is resolved in the proposed study, defining a biased dissimilarity measure between the images.

We suggest a novel framework to *mutual segmentation* of two images of the same object, related by projective transformation. Segmentation is carried out concurrently with registration of the evolving contours. The main contribution of the paper is a construction of two level set functions and a definition of a biased shape dissimilarity measure that accounts for either deficient or excess parts in the images. This measure is also invariant to planar projective transformations. The evolution of each of the level set functions is determined by the gradient descent equations derived by minimizing a region-based and edge-based cost functional. The functional formulation is based on [3, 13, 18] and extended to include the shape dissimilarity term. The outcomes of the proposed algorithm include segmentation of the object appearances in both images and the recovery of the transformation between the object views.

2. Statistical set up and previous art

2.1. General

Segmentation can be formulated via Bayesian statistical inference framework. Given an image $I(x)$ we would like to infer the delineating curve C between an object and its background. This is done via the maximization of the probability distribution function (PDF) $P(C|I)$, using Bayes law:

$$P(C|I) \propto P(I|C)P(C) .$$

The maximization over all possible delineating curves is done by minimizing $-\log P(C|I)$.

Chan and Vese algorithm [3] that we briefly review next presents a prototype for the construction of C when $P(C)$ depends "syntactically" on the internal geometry of the curve. In the level set framework for curve evolution [17], an evolving curve $C(t)$ is defined as the zero level of a level set function $\phi \colon \Omega \to \mathbb{R}$ at time t:

$$C(t) = \{\mathbf{x} \in \Omega | \ \phi(\mathbf{x}, t) = 0\}. \tag{1}$$

Following [3], the Heaviside function of ϕ

$$H(\phi(t)) = \begin{cases} 1 & \phi(t) \geq 0 \\ 0 & \text{otherwise} \end{cases} \tag{2}$$

is used to indicate the object-background regions in the image that correspond the non-negative and negative levels in

ϕ, respectively. Practically, a smooth approximation of the Heaviside function H_ϵ is used [3]:

$$H_\epsilon(\phi) = \frac{1}{2}(1 + \frac{2}{\pi} \arctan(\frac{\phi}{\epsilon})) \tag{3}$$

We can now rephrase our PDF as

$$P(\phi|I) \propto P(I|\phi)P(\phi) .$$

Next, we elaborate on the different terms.

2.2. Region-based data term

Let $I \colon \Omega \to \mathbb{R}^+$ denote a gray level image, where $\Omega \subset \mathbb{R}^2$ is the image domain. Let ω be an open subset of Ω. In the spirit of the Mumford-Shah observation [16], we define a boundary $C \in \Omega$, $C = \partial\omega$ that delimits homogeneous regions in I. Thus, for a general feature $G(I)$ and in the particular case of the two-phase formalism, we look for a curve C that maximizes the difference between two scalars u_+ and u_- defined as follows:

$$u_+ = A^+ \int_\omega G^+(I(\mathbf{x}))d\mathbf{x} \quad u_- = A^- \int_{\Omega\backslash\omega} G^-(I(\mathbf{x}))d\mathbf{x} \tag{4}$$

where $\mathbf{x} \equiv (x, y)$, $A^+ = 1/\int_\omega d\mathbf{x}$ and $A^- = 1/\int_{\Omega\backslash\omega} d\mathbf{x}$. The feature chosen depends on the image homogeneity. In the work of Chan and Vese [3] the image is approximated by a piecewise constant function whose values are given by $G^+(I(x)) = G^-(I(x)) = I(x)$. Hence $u_+ = \overline{I_{in}}$ and $u_- = \overline{I_{out}}$ are the average gray levels in the object regions and in the background regions respectively. For texture segmentation the Gabor filters may be used as in [24] and in [23]. In this study we use the average gray level and the variance:

$$G^+(I) = (I(\mathbf{x}) - \overline{I_{in}})^2 \quad G^-(I) = (I(\mathbf{x}) - \overline{I_{out}})^2 \tag{5}$$

This was considered by [27] and by [15] in the past. We may now express the term $-\log P(I|\phi)$ via a region based cost functional with a well defined integration domain:

$$\begin{aligned} E_{RB}(\phi) = & \int_\Omega \big[(G^+(I(\mathbf{x})) - u_+)^2 H_\epsilon(\phi) \\ & + (G^-(I(\mathbf{x})) - u_-)^2(1 - H_\epsilon(\phi))\big]d\mathbf{x} \end{aligned} \tag{6}$$

The evolving boundary $C(t)$ is derived from $\phi(t)$ using (1). For a given $\phi(t)$ and G the scalars u_+ and u_- should be updated at each iteration according to (4). The level set function ϕ should be updated using its first variation:

$$\phi_t^{RB} = \delta_\epsilon(\phi)\big[G^-(I(\mathbf{x})) - u_-)^2 - (G^+(I(\mathbf{x})) - u_+)^2\big] \tag{7}$$

The evolution of ϕ at each time steps is weighted by the derivative of the regularized form of the Heaviside function:

$$\delta_\epsilon(\phi) = \frac{dH_\epsilon(\phi)}{d\phi} = \frac{1}{\pi}\frac{\epsilon}{\epsilon^2 + \phi^2}.$$

2.3. Edge-based data term

2.3.1 Geodesic active contour: data part

Edge based segmentation approaches usually define the object boundaries by the local maxima of the image gradients. Let $C(s) = (x(s), y(s))$ be the parametric description of a planar contour $C : [0, L] \rightarrow \mathbb{R}^2$ where s is an arc-length parameter.

Let $\nabla I(x, y) = (I_x, I_y)^T = \left(\frac{\partial I(x,y)}{\partial x}, \frac{\partial I(x,y)}{\partial y} \right)^T$ denote the vector field of the image gradients. We will unorthodoxly split the Geodesic Active Contours (GAC) [2] term into two terms. The data term (DCGAC) is given by

$$E_{DGAC}(C) = \int_\Omega \tilde{g}_{DGAC}(C(s)) ds \qquad (8)$$

where

$$\tilde{g}_{DGAC}(\mathbf{x}) = -\frac{|\nabla I|^2}{1 + |\nabla I|^2} \ . \qquad (9)$$

This term vanishes as the gradient magnitudes decrease to zero and attains -1 asymptotically for large gradients. Clearly the curve that minimizes the functional passes through points of high gradient magnitudes.

Expressing this term in a level-set framework we obtain

$$E_{DGAC} = \int_\Omega \tilde{g}(|\nabla I|) |\nabla H_\epsilon(\phi(\mathbf{x}))| d\mathbf{x}, \qquad (10)$$

with the associated gradient descent equation:

$$\phi_t^{DGAC} = \delta_\epsilon(\phi) \mathrm{div} \left(\tilde{g}(|\nabla I|) \frac{\nabla \phi}{|\nabla \phi|} \right). \qquad (11)$$

The GAC functional includes another geometrical term that will be described in subsection 2.4.

2.3.2 Alignment term

The geodesic active contour term (10) determines the location of the zero level of ϕ. Segmentation can be refined by constraining the level set normal direction to align with the image gradient direction as suggested in [26] and independently in [13]. The robust alignment term (RA) defined in [12] takes the form: $E_{RA}(C) = \int_0^L |\langle \nabla I(\mathbf{x}(s)), \vec{n}(s) \rangle| \, ds$, where $< \cdot, \cdot >$ denotes an inner product and $\vec{n}(s) = \{-y_s(s), x_s(s)\}$ is the exterior normal to the curve C. The expression for $E_{RA}(C)$ is an integration of the projection of ∇I on the pointwise normal $\vec{n}(s)$ along the curve. A minor contribution of this paper is the level-set formulation of the alignment term:

$$E_{RA} = \int_\Omega \left| \langle \nabla I, \frac{\nabla \phi}{|\nabla \phi|} \rangle \right| |\nabla H_\epsilon(\phi)| \, d\mathbf{x} \qquad (12)$$

where $\nabla \phi(\mathbf{x})/|\nabla \phi(\mathbf{x})|$ is normal to the level-set ϕ in $\mathbf{x}$. The associated gradient descent equation is

$$\phi_t^{RA} = \delta_\epsilon(\phi) sign(< \nabla \phi, \nabla I >) \Delta I. \qquad (13)$$

This equation is similar to the one derived in [12].

2.4. Syntactic prior: Geometry

The curve length $|C|$ is described by the parametric representation of the curve: $\int_0^L C(s) ds$. An equivalent representation, using the level set formulation takes the form:

$$|C| = E_{LEN} = \int_\Omega |\nabla H(\phi(\mathbf{x}))| d\mathbf{x} \qquad (14)$$

This functional measure the length of the curve and usually serves as an indicator for the curve smoothness [3]. Minimizing (14) with respect to ϕ, we obtain the associated Euler Lagrange equation for ϕ:

$$\phi_t^{LEN} = \delta_\epsilon(\phi) \mathrm{div} \left(\frac{\nabla \phi}{|\nabla \phi|} \right). \qquad (15)$$

Combining E_{LEN} and E_{DGAC} (Eq.(10)), we get the usual form of the GAC functional [11, 2],

$$E_{GAC} = \int_\Omega g(|\nabla I|) |\nabla H_\epsilon(\phi(\mathbf{x}))| d\mathbf{x}, \qquad (16)$$

with the gradient descent equation:

$$\phi_t^{GAC} = \delta_\epsilon(\phi) \mathrm{div} \left(g(|\nabla I|) \frac{\nabla \phi}{|\nabla \phi|} \right). \qquad (17)$$

Here $g = 1 + \tilde{g} = 1/(1 + |\nabla I|^2)$.

2.5. Semantic prior: Shape Term

The edge-based, region-based and smoothness constraints are integrated to establish the following cost functional for segmentation:

$$E_{CVK}(\phi) = E_{RB} + E_{LEN} + E_{GAC} + E_{RA} \qquad (18)$$

with the equations (6, 14, 16, 12). The evolution of ϕ in each time step, $\phi(t+1) = \phi(t) + \phi_t$ is determined by

$$\phi_t(\phi) = \phi_t^{RB} + \phi_t^{LEN} + \phi_t^{GAC} + \phi_t^{RA} \qquad (19)$$

where each contribution to the sum ϕ_t is normalized to $[-1, 1]$. Note that the priors here are "syntactic" and not "semantic" since they control the curve form and do not specifically relate to a certain object or object class. Semantic prior, if available, can significantly facilitate the segmentation process. Denoting a given prior curve by C_p, the statistical formulation is then

$$P(C, T|I, C_p) \propto P(I|C) P(C|C_p, T) P(T)$$

where T is the alignment term between C and C_p.

Let $\tilde{\phi}\colon \Omega \to \mathbb{R}$ denote a prior shape representation. We now review several dissimilarity measures $D(\phi, \tilde{\phi})$ between shape representations $\tilde{\phi}$ and ϕ. When $\tilde{\phi}$ is a distance function and is **aligned** with ϕ a natural choice would be:

$$D(\phi, \tilde{\phi}) = \int_\Omega \left(\phi(\mathbf{x}) - \tilde{\phi}(\mathbf{x}) \right)^2 d\mathbf{x}.$$

This measure, however, depends on the integration domain Ω, see [6] and references therein. Moreover, in a cluttered image, when the weight of this measure in the segmentation functional is high, objects that do not correspond to the prior shape are ignored [7]. To avoid these drawbacks several modifications to control the integration domain have been suggested [6, 7, 22]. Usually, an alignment function between ϕ and $\tilde{\phi}$ is introduced in D. Note that by setting ϕ to be a distance function only isometries (similarity transformations) can be accommodated.

Recently, [19] suggested to use the square difference between the Heaviside functions of ϕ and $\tilde{\phi}$ as a dissimilarity measure between the shape representations, where ϕ and $\tilde{\phi}$ are **not** distance functions.

$$D(\phi, \tilde{\phi}) = \int_\Omega \left[H_\epsilon(\phi(\mathbf{x})) - H_\epsilon(T_p(\tilde{\phi}(\mathbf{x}))) \right]^2 d\mathbf{x} \quad (20)$$

This formulation enables the introduction of the projective alignment term T_p between the shapes. Furthermore, D does not depend on the integration domain. The shape term (20) is suitable when the prior $\tilde{\phi}$ is perfect and constant in time. However, in the proposed setup when $\tilde{\phi}$ is the evolving (and imperfect) segmentation of the other image, a different dissimilarity measure should be employed.

3. Mutual Segmentation with Projectivity

In this paper we consider the segmentation of two images, I_1 and I_2 that provide two imperfect (occluded, noisy etc.) instances of an object. When a perfect prior C_p is not available the statistical inference problem takes the form:

$$P(C_1, C_2, T | I_1, I_2) \propto P(I_1, I_2 | C_1, C_2) P(C_1 | C_2, T) P(T)$$

The term $P(C_1 | C_2, T)$ is defined via biased shape dissimilarity measure and is discussed next.

3.1. Biased shape dissimilarity measure

Consider the image pair in Figure 1a-b. Both have deficiencies. In Fig. 1a a portion of the creature's left leg was erased. In Fig. 1b the hoop is absent. When the final segmentation of Fig. 1a is the prior for the segmentation of Fig. 1b and vice versa, the imperfections of each segmentation spoil the other, as shown in Fig. 1e-f. Note that the left leg in incorrectly segmented in Fig. 1e, while the hoop in Fig. 1f is not segmented at all.

The images in Fig.1c-d contain superfluous hoops located in different places. When each segmentation is the prior for the other, using the unbiased dissimilarity measure in Eq. (20), the contours of the superfluous hoops in Fig.1c-d undesirably appear in the segmentation shown in Fig.1h,g respectively.

The distinction between integral object parts (leg, hoop) and other surrounding objects (superfluous hoops) raises a fundamental question which extends beyond the scope of the current work and relates to perceptual organization of images in general. Given more than two images, this difficulty can be tackled by employing a majority rule to enhance the final object-background labeling. However, for mutual segmentation of two images another decision tool or source of information is needed. For simplicity, we assume either of the following "world states":

1. **The images to segment have (mostly) deficiencies.** When this rule is applied for Fig. 1a-b the creature's leg will be reconstructed and the hoop would be well segmented, as shown in Fig. 1i-j.

2. **The images to segment have (mostly) excess parts.** When this rule is applied for Fig. 1c-d the superfluous hoops are labeled as background as in Fig. 1k-l.

3. **The prior shape is perfect.** Examples for the application of this rule are shown in Fig. 1e-h.

Refer again to the dissimilarity measure in Eq. (20). The cost functional integrates the non-overlapping object-background regions in both images indicated by $H_\epsilon(\phi)$ and $H_\epsilon(\tilde{\phi})$. This is equivalent to a pointwise exclusive-or (xor) operation integrated over the image domain. We may thus rewrite the functional as follows:

$$D(\phi, \tilde{\phi}) = \int_\Omega \left[H_\epsilon(\phi) \left(1 - H_\epsilon(\tilde{\phi}_T) \right) \right. \\ \left. + \left(1 - H_\epsilon(\phi) \right) H_\epsilon(\tilde{\phi}_T) \right] d\mathbf{x} \quad (21)$$

To simplify the expression we denote $T_p(\tilde{\phi}) \equiv \tilde{\phi}_T$. Note that the expressions (20) and (21) are approximately identical, since $H_\epsilon(\phi) \approx (H_\epsilon(\phi))^2$ (equality is obtained for $\epsilon \to 0$). There are two types of disagreement between the labeling of $H(\phi)$ and $H(\tilde{\phi}_T)$. The left term in (21) does not vanish if there exist image regions labeled as *object* by the image data (ϕ) and labeled as *background* by the shape prior ($\tilde{\phi}_T$). The right term in (21) does not vanish if there exist image regions labeled as *background* by the image data and labeled as *object* by $\tilde{\phi}_T$. Inserting a weight parameter $\mu \geq 0$, the relative contributions of the terms is changed.

$$E_S(\phi, \tilde{\phi}) = \int_\Omega \left[\mu H_\epsilon(\phi) \left(1 - H_\epsilon(\tilde{\phi}_T) \right) \right. \\ \left. + \left(1 - H_\epsilon(\phi) \right) H_\epsilon(\tilde{\phi}_T) \right] d\mathbf{x} \quad (22)$$
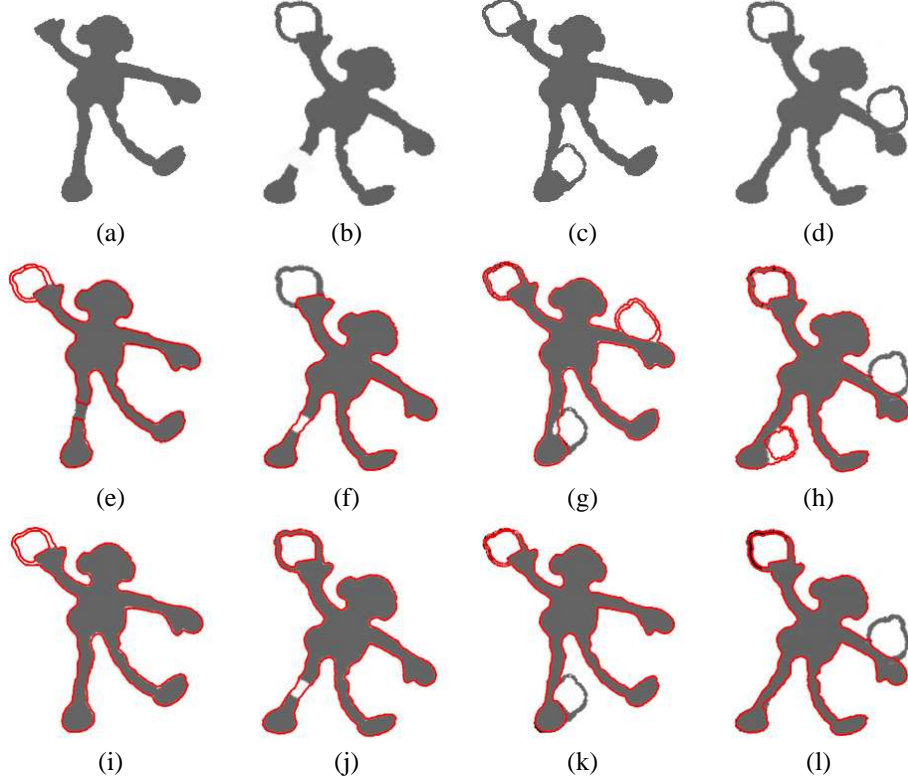
Figure 1. (a)-(b) Input images with deficiencies. (c)-(d) Input images with excess parts. (e) Segmentation (red) of the image in (a) using (b) as a prior. (f) Segmentation of the image in (b) using (a) as a prior. (g) Segmentation of the image in (c) using (d) as a prior. (h) Segmentation of the image in (d) using (c) as a prior. (i)-(j) Mutual segmentation results for images (a) and (b) respectively. (k)-(l) Mutual segmentation results for images (c) and (d) respectively. The images are related by projective transformation. The recovered parameters are shown and compared in Table 1.

Homography ratios	$\hat{h_1}$	$\hat{h_2}$	$\hat{h_3}$	$\hat{h_4}$	$\hat{h_5}$	$\hat{h_6}$	$\hat{h_7}$	$\hat{h_8}$
$\mathcal{H}_{1\to2}$	0.990	-0.417	0.3607	0.320	0.902	29.08	0.0005	0.0007
$\mathcal{H}_{1\to2}^{-1}$	0.858	0.406	-12.12	-0.298	0.964	-27.93	-0.0002	-0.0009
$\mathcal{H}_{2\to1}$	0.868	0.408	-12.11	-0.302	0.969	-27.90	-0.0001	0.0009

Table 1. Comparison of the homography matrix entries obtained through the registration phase in the mutual segmentation algorithm applied to Fig. 1. Compare the values of $\mathcal{H}_{2\to1}$ to $\mathcal{H}_{1\to2}^{-1}$

The associated gradient equation for ϕ is then:

$$\phi_t = \delta_\epsilon(\phi)[H(\tilde{\phi}_T) - \mu(1 - H(\tilde{\phi}_T))] \qquad (23)$$

Now, if excess parts are assumed the left penalty term should be dominant thus $\mu > 1$. Otherwise, if deficiencies are assumed the right penalty term should be dominant and $\mu < 1$.

3.2. Projective invariance

Let I_1 and I_2 be two images of the same object related by planar projective transformation T_p. Let $p \in I_1$ and $p' \in I_2$ denote corresponding image points. Their coordinates $\mathbf{x}$ and $\mathbf{x}'$ are related by planar projective homography, i.e.

$\mathbf{x}' = \mathcal{H}\mathbf{x}$ where,

$$\mathcal{H} = \begin{bmatrix} h_{11} & h_{12} & h_{13} \\ h_{21} & h_{22} & h_{23} \\ h_{31} & h_{32} & h_{33} \end{bmatrix} \in \mathbb{R}^{3\times3} \qquad (24)$$

is the Homography matrix. Specifically,

$$x' = \frac{h_{11}x + h_{12}y + h_{13}}{h_{31}x + h_{32}y + h_{33}}, \quad y' = \frac{h_{21}x + h_{22}y + h_{23}}{h_{31}x + h_{32}y + h_{33}} \qquad (25)$$

The eight unknown ratios of the homography matrix entries, $\hat{h_k} = h_{ij}/h_{33}$ are recovered through the segmentation process for each of the pairs $\{\phi_i, T_p(\tilde{\phi}_i)\}$, where

$T_p(\tilde{\phi}(\mathbf{x})) = \tilde{\phi}(\mathbf{x}')$, $\mathbf{x}' = (x, y)$. The PDEs for $\hat{h}_k$ are obtained by minimizing (22) with respect to each.

$$\frac{\partial \hat{h}_k}{\partial t} = 2 \int_\Omega \delta_\epsilon(T_p(\tilde{\phi})) \left[(1 - H_\epsilon(\phi)) - \mu H_\epsilon(\phi) \right] \frac{\partial T_p(\tilde{\phi})}{\partial \hat{h}_k} d\mathbf{x} \tag{26}$$

Derivation of $\frac{T_p(\tilde{\phi})}{\partial \hat{h}_k} d\mathbf{x}$ can be done similarly to [20].

3.3. Algorithm

We summarize the proposed algorithm assuming the following setup. The input is two images I_1 and I_2 of the same object, taken from a different point. Object contours are approximately coplanar. For each image I_i alternately carry out the following:

1. Choose an initial level-set function ϕ_i, for example a standard circular (or elliptic) cone. Its zero level-set should form an initial contour within the image.

2. Set initial values (e.g. zero) for the transformation parameters $\hat{h}_k$.

3. Compute the values u_+ and u_- using Eq. (4), based on the current object-background regions, defined by $\phi(t)$.

4. The prior representation is determined by the level set function of the other image: $\tilde{\phi}_i = \phi_j$, $i, j = \{1, 2\}$, $i \neq j$.

5. Transform the prior shape representation, applying $\tilde{\phi} \rightarrow T_p(\tilde{\phi})$ using (25) with the estimated parameters of the preceding time step.

6. Update ϕ using the gradient descent equation (23).

7. Update the transformation parameters h_k using the derivatives (26). The relation $\mathcal{H}_1 = \mathcal{H}_2^{-1}$ can be used either for verification or to speed up the recovery of the parameters.

8. Repeat steps 3-7 until convergence.

4. Experiments

We exemplify the mutual segmentation algorithm on image pairs related by projective transformations. The input images are shown with the initial and final segmenting contours. The mismatch between the respective object views is demonstrated by superposition of the images. The accuracy of independently recovered homographies $\mathcal{H}_{i \rightarrow j}$ between image i and image j is verified using the relation $\mathcal{H}_{i \rightarrow j} = \mathcal{H}_{j \rightarrow i}^{-1}$. Table 1 exemplifies such comparison relates to Fig. 1. In all the experiments we set $dt = 0.1$ and

$\epsilon = 1$. Normalizing the contributions of each gradient descent equation of ϕ in (7) to $[-1, 1]$, we avoided the cumbersome task of tuning the relative weight parameters. Figure 2 shows two images of a hand taken from two different view points. The misalignment between the hand instances is shown in Fig. 2e. A successful segmentation of both images are demonstrated in Fig. 2c-d, setting $\mu < 1$. Fig. 2f-h demonstrate unsuccessful segmentation of each image by itself. The noisy image has been segmented twice Fig. 2g-h for different weights of the contour smoothness term. In Fig. 2h the contour is smoother, yet it does not extract precisely the fingers.

The boot images in Fig. 3a-b were mutually segmented using the proposed algorithm, with $\mu < 1$. The delineating contour (shown in Figure 3d-e) traces precisely the boot boundaries while completing correctly the occluded parts. The misalignment between the boot instances is shown in Fig. 3c. Fig. 4a-b demonstrates mutual segmentation of two images of a license plate with corrupted digits. Assuming excess parts we set $\mu > 1$. For a comparison, fig. 4c-d display undesired segmentation results obtained when each image is segmented by itself.

5. Discussion

We presented a method for concurrent, mutually-supporting segmentation of two images of the same object, taken from different view points. Having *two* images instead of one provides redundancy that is employed by using each instance to guide the segmentation of the other. Unlike previous methods, the concept of a perfect shape prior is replaced by information gathered from incomplete instances.

Segmentation is metaphorically similar to cliff climbing. Prior-based segmentation is analogous to situations where someone climbs first and secures a rope to the cliff. If this is not possible, the combined effort of at least a duo is needed. The two climb in turns: at each stage one person holds the cliff and helps the other climb. The main contribution of this paper is the formulation of this duo shape term, that enables solution of the mutual segmentation problem.

Having two images of the same object is helpful in regions where the aligned images agree, but there is an inherent ambiguity where they don't. In this paper, we address this ambiguity via the biased shape dissimilarity measure. Note that if more than two images are available, the ambiguity can be resolved by a majority rule. This is a topic for future research.

Acknowledgment
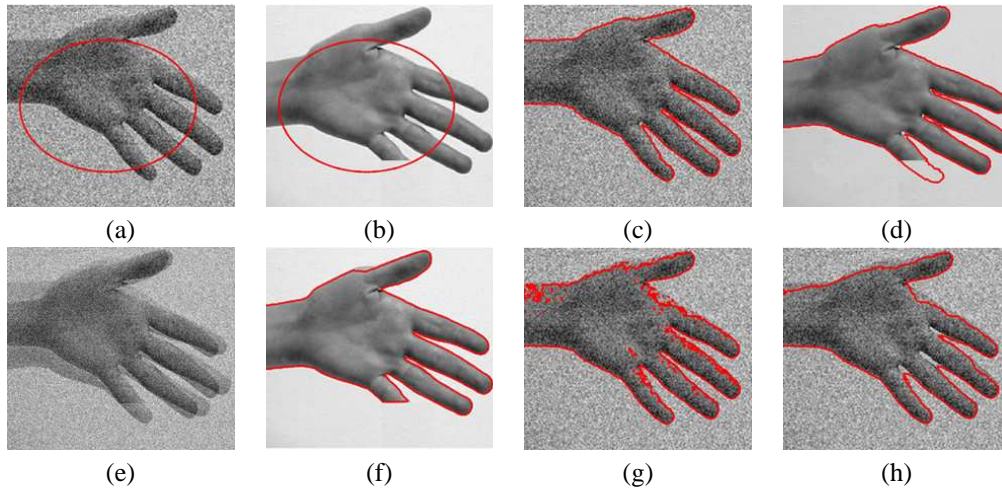
Figure 2. (a)-(b) Input images with their initial contours (red). (c)-(d) Successful mutual segmentation results (red). (e) Superposition of the two images to demonstrate the misalignment. (f)-(h) Segmentation of each image by itself. The noisy image has been segmented twice with different weights of smoothness term: (g) The contour "mistakenly" follows image gradients that are due noise. (h) Segmentation with high smoothness term. The contour is smooth but the fingers are not well extracted.
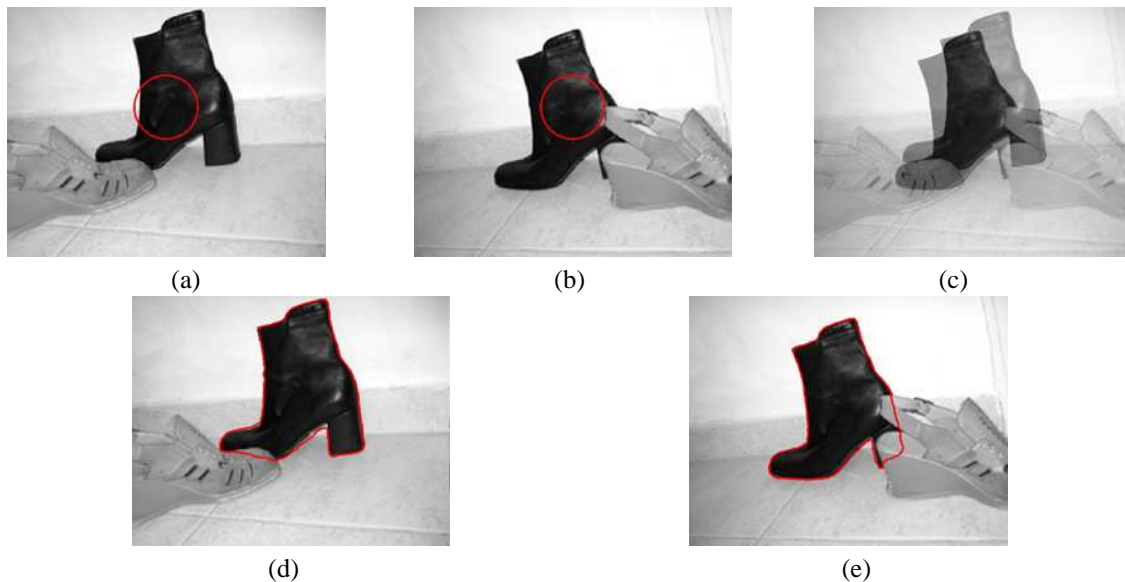
Figure 3. (a)-(b) Input images with their initial contours (red). (c) Superposition of the two images to demonstrate the misalignment. (d)-(e) Successful mutual segmentation results (red).

References

[1] G. Aubert and P. Kornprobst. *Mathematical Problems in Image Processing: Partial Differential Equations and the Calculus of Variations*. Springer, 2002.

[2] V. Caselles, R. Kimmel, and G. Sapiro. Geodesic active contours. *IJCV*, 22(1):61–79, Feb. 1997.

[3] T.F. Chan and L.A. Vese. Active contours without edges. *IP*, 10(2):266–277, Feb. 2001.

[4] Y. Chen, H.D. Tagare, S. Thiruvenkadam, F. Huang, D. Wilson, K.S. Gopinath, R.W. Briggs, and E.A. Geiser. Using prior shapes in geometric active contours in a variational framework. *IJCV*, 50(3):315–328, Dec. 2002.

[5] D. Cremers, T. Kohlberger, and C. Schnörr. Shape statistics in kernel space for variational image segmentation. *Pattern Recognition*, 36(9):1929–1943, 2003.

[6] D. Cremers and S. Soatto. A pseudo-distance for

Figure 4. (a)-(b)Successful Mutual segmentation of license plate images with corrupted digits taken from 2 viewpoints.(c)-(d) Segmentation of each license plate image by itself using the Chan-Vese level-set method for segmentation.

shape priors in level set segmentation. In *VLSM*, pages 169–176, 2003.

[7] D. Cremers, N. Sochen, and C. Schnörr. Multiphase dynamic labeling for variational recognition-driven image segmentation. *IJCV*, 2005.

[8] A. Duci, A. Yezzi, S. Mitter, and S. Soatto. Region matching with missing parts. In *ECCV*, volume 3, pages 48–64, May 2002.

[9] M. Holtzman-Gazit, R. Kimmel, N. Peled, and D. Goldsher. Segmentation of thin structures on volumetric medical images. *IP*, 15(2):354–363, 2006.

[10] X. Huang, Z. Li, and D. Metaxas. Learning coupled prior-shape and appearance models for segmentation. In *MICCAI*, volume I, pages 60–69, 2004.

[11] Satyanad Kichenassamy, Arun Kumar, Peter J. Olver, Allen Tannenbaum, and Anthony J. Yezzi. Gradient flows and geometric active contour models. In *ICCV*, pages 810–815, 1995.

[12] R. Kimmel. Fast edge integration. In S. Osher and N. Paragios, editors, *Geometric Level Set Methods in Imaging Vision and Graphics*. Springer-Verlag, 2003.

[13] R. Kimmel and A.M. Bruckstein. Regularized laplacian zero crossings as optimal edge integrators. *IJCV*, 53(3):225–243, 2003.

[14] M.E. Leventon, W.E.L. Grimson, and O. Faugeras. Statistical shape influence in geodesic active contours. In *CVPR*, volume I, pages 316–323, 2000.

[15] L.M. Lorigo, O. Faugeras, Grimson W.E.L., R. Keriven, R. Kikinis, A. Nabavi, and C.F. Westin. Codimension two-geodesic active contours for the segmentation of tabular structures. In *CVPR*, pages 444–451, 2000.

[16] D. Mumford and J. Shah. Optimal approximations by piecewise smooth functions and associated variational problems. *Communications on Pure and Applied Mathematics*, 42:577–684, 1989.

[17] S. Osher and J.A. Sethian. Fronts propagating with curvature-dependent speed: Algorithms based on Hamilton-Jacobi formulations. *Journal of Computational Physics*, 79:12–49, 1988.

[18] N. Paragios and R. Deriche. Geodesic active regions: A new paradigm to deal with frame partition problems in computer vision. *Journal of Visual Communication and Image Representation*, 13:249–268, 2002.

[19] T. Riklin-Raviv, N. Kiryati, and N. Sochen. Unlevelsets: Geometry and prior-based segmentation. In *ECCV*, volume 4, pages 50–61, 2004.

[20] T. Riklin-Raviv, N. Kiryati, and N. Sochen. Prior-based segmentation by projective registration and level-sets. In *ICCV*, pages 204–211, 2005.

[21] M. Rochery, I.H. Jermyn, and J. Zerubia. Higher-order active contours. *IJCV*. to appear.

[22] M. Rousson and N. Paragios. Shape priors for level set representation. In *ECCV*, pages 78–92, 2002.

[23] C. Sagiv, N. Sochen, and Y.Y. Zeevi. Integrated active contours for texture segmentation. *IP*. to appear.

[24] B. Sandberg, T. Chan, and L. Vese. A level-set and gabor based active contour for segmenting textured images. Technical report, UCLA CAM report, 2002.

[25] A. Tsai, A. Yezzi, Jr., W.M. Wells, III, C. Tempany, D. Tucker, A. Fan, W.E.L. Grimson, and A.S. Willsky. A shape-based approach to the segmentation of medical imagery using level sets. *IEEE Trans. on Medical Imaging*, 22(2):137–154, 2003.

[26] Alexander Vasilevskiy and Kaleem Siddiqi. Flux maximizing geometric flows. In *ICCV*, pages 149–154, 2001.

[27] L.A. Vese and T.F. Chan. A multiphase level set framework for image segmentation using mumford and shah model. *IJCV*, 50(3):271–293, 2002.

[28] A. Yezzi, L. Zöllei, and T. Kapur. A variational framework to integrate segmentation and registration through active contours. *Medical Image Analysis*, 7:171–185, 2003.